Title

Microfluidic Printing-Based Method for the Multifactorial Study of Cell-Free Protein Networks

Journal

Analytical Chemistry, 94(31)

ISSN

0003-2700

Authors

Zhou, Chuqing

Shim, Jiyoung

Fang, Zecong

et al.

Publication Date

2022-08-09

DOI

10.1021/acs.analchem.2c01851

Peer reviewed

HHS Public Access

Author manuscript

Anal Chem. Author manuscript; available in PMC 2023 August 09.

Published in final edited form as:

Anal Chem. 2022 August 09; 94(31): 11038–11046. doi:10.1021/acs.analchem.2c01851.

A microfluidic printing based method for the multifactorial study of cell-free protein networks

Chuqing Zhou[1,#], **Jiyoung Shim**[1,#], **Zecong Fang**[2,3], **Conary Meyer**[1], **Ting Gong**[1], **Matthew Wong**[1], **Cheemeng Tan**[1,*], **Tingrui Pan**[2,3,4,5,*]

[1]Department of Biomedical Engineering, University of California, Davis, California, 95616, USA

[2]Institute of Biomedical and Health Engineering, Shenzhen Institute of Advanced Technology, Chinese Academy of Science, Shenzhen, 518055, China.

[3]Shenzhen Engineering Laboratory of Single-Molecule Detection and Instrument Development, Shenzhen, Guangdong, 518055, China.

[4]Suzhou Institute for Advanced Research, University of Science and Technology of China, Suzhou, 215123, China.

[5]Department of Precision Machinery and Precision Instrumentation, University of Science and Technology of China, Hefei, 230026, China.

Abstract

Protein networks can be assembled in vitro for basic biochemistry research, drug screening, and the creation of artificial cells. Two standard methodologies are used: manual pipetting; pipetting robots. Manual pipetting has limited throughput in the number of input reagents and the combination of reagents in a single sample. While pipetting robots are evident in improving pipetting efficiency and saving hands-on time, their liquid handling volume usually ranges from a few to hundreds of microliters. Microfluidic methods have been developed to minimize the reagent consumption and speed up screening, but are challenging in multifactorial protein studies due to their reliance on complex structures and labeling dyes. Here, we engineered a new impact-printing-based methodology to generate printed microdroplet arrays containing water-in-oil droplets. The printed droplet volume was linearly proportional (R^2=0.9999) to the single droplet number, and each single droplet volume was around 59.2 nL (Coefficient of Variation=93.8%). Our new methodology enables the study of protein networks in both membrane-unbound and -bound states, without and with anchor lipids DGS-NTA(Ni) respectively. The methodology is

*corresponding authors: Cheemeng Tan (cmtan@ucdavis.edu) and Tingrui Pan (tingrui@ustc.edu.cn).
#Chuqing Zhou and Jiyoung Shim contributed equally.

Author contribution

C.Z. integrated the microfluidic robot, fabricated the microfluidic cartridge, characterized the droplet size, performed the quantification of fluorescent protein immobilization and wrote the related parts of the manuscript, J.S. and Z.F. aided in these parts of writing; J.S. expressed and purified MEK1 (R4F) *, pERK2, and ERK2, verified their activities using well-plate and western blotting-based assay, and wrote the related parts of the manuscript; C.Z. and J.S. designed and performed multiplexed droplet screening of their activites (MEK1 * and –ERK2), C.Z. wrote the codes for processing fluorescent images, J.S. analyzed the data and wrote the related parts of the manuscript; Z.F. and C.M. helped improve the robustness of the microfluidic robot; T.G. helped prepare the lipid-containing oil; M.W. assisted with the study of the His-tagged GFP; C.T. and T.P. planned the project, designed and supervised the experiments, and revised the manuscript.

Conflicts of interest

There are no conflicts to declare.

demonstrated using a sub-network of mitogen-activated protein kinase (MAPK). It takes less than 10 minutes to prepare 100 different droplet-based reactions, using < 1 μL reaction volume at each reaction site. We validate the kinase (ATPase) activity of MEK1 (R4F) * and ERK2 WT individually and together under different concentrations, without and with the selective membrane attachment. Our new methodology provides a reagent-saving, efficient and flexible way for protein network research and related applications.

Graphical Abstract

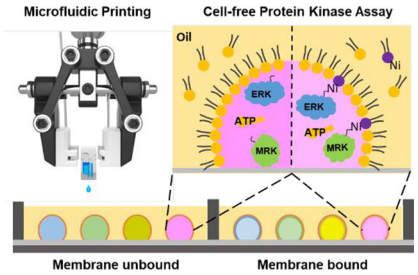

Keywords

protein network; *in vitro* ; microfluidic printing; ATPase activity; signal transduction

Introduction

Recent work has reconstituted protein networks *in vitro*, where at least two purified catalytic compounds (enzymes and proteins) are put together to investigate how they affect each other and give rise to a cellular function of interest.[1,2] The emerging studies of protein networks are becoming important for various applications, for instance, switching on/off biological transduction pathways[3,4], developing energy self-supplying systems[5,6], and screening peptide-based drugs[7]. Conventionally, the biochemical study of proteins is carried out in multiwell plates, where the reaction volume ranges from a few to hundreds of microliters. Thus, the reagent cost is considerable for quantitative protein network studies that consist of thousands of protein network reactions. In addition, the well plate-based methods have intrinsic fundamental limitations for the assembly of the protein network. As revealed recently, protein kinase reactions in solution (well plate-based) is different from that in droplet-based vesicles, mainly due to the membrane confinement or attachment.[3,8,9]

To minimize the reagent consumption and speed up screening, droplet microfluidics is emerging as a powerful tool for the construction of droplet-based protein assays.[10–12] Weitz's group has developed a droplet-based ultrahigh-throughput screening platform to discover variants of the enzyme horseradish peroxidase (HRP).[13] In another example, Kennedy's group has demonstrated a label-free screening of inhibitors for cathepsin B using microfluidic droplet-based electrospray ionization mass spectrometry.[14] To extend the time of reaction monitoring, static microdroplet arrays could be formed on chip using microfluidic trapping structure.[15–17] Recently, efforts have been made on the encapsulation of multiple biomolecular reagents in water-in-oil droplets in micrometer-sized compartments as the next-generation platform for the construction of artificial cells.[18,19] For instance, a

cross junction-based microfluidic design has been successfully used for the encapsulation of hybrid synthetic chloroplasts[5] and DNA fragments with the IVT2H reagents[7] in droplets in high throughput. Furthermore, a six-way junction-based droplet-generating device has been demonstrated for the study of a three-enzyme (β-gal, GOx, and HRP) combinatorial biochemical pathways.[1] Such studies have validated the benefits of reconstituting biological pathways using droplet microfluidics, demonstrating features such as high-frequency, high encapsulation efficiency, and precise size control.

Meanwhile, it remains challenging for conventional droplet microfluidic devices to flexibly vary the droplet contents on demand.[20,21] To this end, picoliter/nanoliter injection technologies have been lately employed for combinatorial screening applications. For instance, Weiss and his co-workers have designed injection channels downstream of a vesicle-encapsulation channel. They used a high voltage to induce the fusion of the reagent from the injection channel into the vesicle, and they have successfully tuned the injected volume by varying the pressure in the injection channel.[19–20] In another example, Rane's group has employed a valve-based droplet generation method for reagent injection and droplet displacement operations in a microfluidic device, and they have adjusted the reagent injection volume and concentration in a droplet by tuning the duration of valve opening.[20] However, such on-chip injection devices need to monitor different droplets using techniques such as injecting labeling reagents or designing a lengthy incubation channel. To address this problem, Cole and his co-workers have developed printed droplet microfluidics that enables the dispensing of desired droplets in an arrayed format on an oil-moat substrate.[23] However, extra efforts are still required to distinguish mixed feed reagents using labeling dyes or designing a complex feed structure. Therefore, the current droplet microfluidics-based platforms are still challenging for the multifactorial studies of protein networks.

Recently, our group has developed a microfluidic printing robot to generate combinatorial microdroplet arrays on a hydrophobic substrate using modular printing heads.[24] Here, based on the published printing robot, we demonstrate a novel approach to perform multifactorial studies of protein networks in microdroplet arrays. In the first step, we utilize our previously developed microfluidic pipette-free robot that incorporated with a robotic-microfluidic interface (RoMI) to handle multiple microfluidic cartridges to generate multiplexed droplet arrays on a hydrophobic substrate, seamlessly integrating the modular microfluidic cartridges with robotic operations for the automated low volume pipetting.[24] Notably, these microfluidic cartridges are inexpensive and disposable, with an accuracy of 93.8% in generating 59.2 nL single droplets. In the second step, phospholipid-dissolved oil is poured over the droplet arrays to form a lipid membrane surrounding the preformed droplets. In addition, anchor lipids DGS-NTA(Ni) are selectively added into the oil, allowing for the specific bindings between the lipid membrane and his-tagged proteins inside the preformed droplet. As a demonstration, we assemble a sub-network of mitogen-activated protein kinase (MAPK) containing MEK or/and ERK kinase. Around 100 droplets with different protein concentrations have been prepared within 10 min, in which the droplet size (1 μL) is 1–2 orders of magnitude lower than that of the conventional well plate-based protein network reactions. We also study the activities of both unbound and bound kinases simultaneously. We confirm that protein networks study could be carried out on printed

microdroplet arrays, and the system provides a reagent-saving, efficient and flexible way for protein network research and related applications.

Methods

M1: Microfluidic Printing Robot Integration

Microfluidic printing robot was built on a 4-DoF robotic arm (Magician, Dobot, Shenzhen, China). The robot arm was integrated with a pressure controller (PG-MFC, PreciGenome, San Jose, CA) and a custom-made valve controller. The valve controller was based on Arduino architecture with two mini solenoid valves (LHDA1221111H, Lee Co, Franklin, TN). The robotic arm was equipped with a two-finger gripper that applied a horizontal force using an embedded air pump in the robot. A pair of customized 3D-printed connectors were mounted on the robotic gripper that served as a seamless pneumatic connection between the robot and the microfluidic cartridge. As a result, the compressed air could be introduced from the robot to the cartridge controlled by the valve control circuit with the sub-millisecond resolution. The system was communicated and controlled by a computer via USB ports in a programmable manner (Python, Python software foundation, Beaverton, OR). More details of the fully automated liquid handling process have been described in the previous work[24].

M2: Microfluidic Cartridge Fabrication

The microfluidic cartridge consisted of a 3D-printed reservoir/macrochannel layer, a double-adhesive microchannel layer, and a micronozzle layer. The cartridge could store 200 μL of reagent volume in the reservoir. The reservoir/macrochannel layer was designed in SolidWorks software and fabricated with a Clear Resin (Formlabs) using SLA 3D printer (Formlabs Form 3)[25,26]. The double-adhesive microchannel layer (ARcare® 90445, Adhesives Research, thickness of 80 μm) was designed in AutoCAD, and laser-cut (Universal Laser Systems, VersaLaser 2.30) to form the microchannel with a width of 200 μm. The micronozzle layer was fabricated by drilling 80 μm through-holes on a PMMA sheet (Nuowei, Shenzhen, thickness: 75 μm). These three layers were aligned and assembled layer by layer under an inverted stereoscope. More details of the principle of the microfluidic cartridge design have been described in the previous work[24].

M3: Microarray Substrate

Polydimethylsiloxane (PDMS)-coated cover glass (60×48 mm, Gold Seal®, cat. 48404–142, VWR, Radnor, PA) was used as the array substrate. PDMS was prepared using a 10:1 (w/w) mixture of the base to a curing agent (SYLGARD™ 184, Dow Corning), spin-coated on the cover glasses at 1000 r.p.m. for a 90 μm thick layer, and then cured on a hot plate at 120 °C for 1 hour. PDMS served as a hydrophobic substrate for the formation of water-in-oil droplets (water contact angle is >100°)[27].

M4: Multiplexed Water-in-oil Droplet Microarray Formation

Before printing, the humidity was kept at 40%−50% using a humidifier. The printing parameters were set in an Excel file for each reagent, including starting position, row and column distances, row-column matrix, and the number of accumulated droplets. All

fresh reagents were loaded into the reservoir of the microfluidic cartridges through the side inlet by manual pipetting right before printing. Once grabbing the target reagent from the designated position, a calibration step was set to dispense droplets. Thus, we could visualize the performance of the cartridge. After that, the robot executed the printing task instructed by the Excel file. In our test, both row and column distances were set as 3 mm. The total droplet volume in each site was <1 μL for maintaining the droplet shape. A1.5 mm-thickness acrylic sheet (Amazon, Vacaville, CA) and a double adhesive sheet were cut with a laser machine and assembled into the customized-size frame. After printing, we placed the customized frame around the entire printed droplets and added lipid-dissolved oil over the droplets gently. The estimated oil volume was about 25 μL per droplet.

M5: Preparation of lipid-containing oil

Two different types of lipids were purchased from Avanti Polar Lipids (AL, USA), L-α-phosphatidylethanolamine (cat. 840021C, Egg PE), and 1,2-dioleoyl-sn-glycero-3-[(N-(5-amino-1-carboxypentyl) iminodiacetic acid) succinyl] (nickel salt) (cat. 790404C, DGS-NTA(Ni)), which were used without further purification. Paraffin oil was purchased from Fisher Scientific (cat. AC444180250, Waltham, MA). Two different lipids in different concentrations were mixed in small glass vials, dried under a gentle stream of nitrogen, and then kept under a vacuum for roughly 3 hours. Completely dried lipids were resuspended in the paraffin oil, followed by shaking (200 r.p.m.) at 30 °C overnight. The final concentration of Egg PE was 0.5 mM, while 0–0.1 mM DGS-NTA(Ni) were selectively added for different tests. The dissolved lipids in paraffin oil remained stable at room temperature for around one week.

M6: Droplet Characterization

The printed droplet volume was characterized by the methods of imaging and weighing analysis. The images of droplets were taken under a bright field microscope (EVOS XL, Life Technologies, USA). The diameters of the droplets (on a PDMS array substrate in Figure 2a) were measured through the particle analysis function in ImageJ software (NIH, Bethesda, MD). We estimated the droplet volume by assuming that each droplet is a hemispherical shape with a contact angle of 109° on the substrate (Figure 2b). We weighed it after dispensing 100–1000 times droplets (Figure 2c–d) into a container with mineral oil under a 4-digital microbalance (Mettler Toledo AB54-S/FACT). In Figure 2c, the printing pressure was consistent, but the total printing number changed. In Figure 2d, the printing pressure was adjusted for printing 100 droplets. Through the weighing analysis, we enabled to characterize the droplet volume and the volume linearity. As shown in Figure 2 c–d, the total printed droplet weight converted to total printed volume according to the water density (0.996 g/mL) and 20% v/v glycerol in water density (1.051 g/mL) and further averaged into a single droplet volume as required.

M7: Fluorescence Protein reagents

For visualizing the protein distribution in the water-in-oil droplet, we purchased recombinant proteins, Aequorea Victoria Green Fluorescent Protein (GFP) His-tag (cat. A42613, Thermo Fisher Scientific, MA) and Cy5-streptavidin (PA45001, GE Healthcare). Both proteins were diluted with a PBS buffer (pH = 7.4) before testing.

M8: MEK1 (R4F) and ERK2 kinases expression

We purchased NpT7–5-Erk2 (cat. 39230, Addgene, MA)[28] for expressing His_6-ERK2, and pET-His_6-ERK2-MEK1_R4F_coexpression plasmid (cat. 39212, Addgene, MA)[29] for expressing phosphorylated ERK2 by co-expressing MEK1_R4F and ERK2. Afterward, we cloned His_6-MEK1_R4F into a pET_15b vector to express it alone. All proteins (ERK2, MEK1_R4F, and phosphorylated ERK2) were expressed in the BL21-DE3 strain of *Escherichia coli* and purified using Ni-NTA resin (cat. 88221, ThermoFisher, MA) individually. Cells were grown in Luria Broth (LB, VWR) at 37 °C with carbenicillin (Sigma) at 100 μg/ml until the O.D.600 reaches 0.6–0.8. At which time 0.5 mM Isopropyl b-D-1-thiogalactopyranoside (IPTG) was added and then further incubated for additional 20 hours at 30 °C. After cell lysate, His_6-tagged proteins were separated using Ni-NTA resin equilibrated in sonication buffer. The protein-bound Ni-NTA resin was washed with wash buffer (buffer A:B = 9:1 / 8:2 included 7mM 2-mercaptoethanol), and protein was eluted in elution buffer (buffer A:B = 2:8 included 7mM 2-mercaptoethanol). Buffer A was composed of 50 mM HEPES, 1M NH_4Cl, and 10 mM $MgCl_2$. Buffer B contained 50 mM HEPES, 500 mM Imidazole ($C_3H_4N_2$), and 10mM $MgCl_2$. Additional purification to remove smaller molecules than 3.5 kDa was proceeded with dialysis using a dialyzing tube (cat. 2115210, Fisher, PA). The protein was dialyzed overnight against the final dialysis buffer contained 50 mM HEPES, 100 mM KCl, 50 mM $C_5H_8KNO_4$, 10 mM $MgCl_2$, and 25% glycerol included 7mM 2-mercaptoethanol. After that, the protein was concentrated using10-kDa Amicon unit (cat. UFC801024, EMD Millipore, MA) at 4000xg for 1 hour at 4°C, and stored at −20 °C. We ensured the purity and protein size by SDS-PAGE. Protein concentration was determined by the protein 660 assay (cat. 22660, ThermoFisher, MA) with the bovine serum albumin standards (cat. 23208, ThermoFisher, MA).

M9: MEK or/and ERK activity assay *in vitro*

We used the PhosphoWorksTM Fluorimetric ADP assay kit (cat. 21655, AAT Bioquest, CA) for assaying MEK-ERK network by monitoring red fluorescence intensity due to the ADP formation. We followed the manufacturer's protocol. Briefly, we added 10 μL of the protein solution to 5μL of ADP Sensor and 10 μL of ADP Sensor Buffer for using a fluorescence microplate reader (Tecan M1000Pro, Männedorf, Switzerland). The protein solution contained: 1 μM MEK_R4F and 2.5 μM ERK2 substrate were separately prepared in the kinase buffer (50 mM Tris/HCl (pH 7.4), 150 mM NaCl, 10 mM $MgCl_2$, and 1 mM ATP)[30]. The mixture (Protein solution, ADP Sensor and Buffer) was added to each well of a black flat-bottom 384-well microplate (cat. 781096, Greiner Bio, NC) and monitored for the red fluorescence at 30 °C with shaking (orbital, 1 min every 5 min) for 2 hours. The excitation and emission wavelengths for the ADP sensor were 540 and 590 nm, respectively. After monitoring red fluorescence intensity, we examined ERK2 phosphorylation by MEK1 (R4F) mutant(*) in the same reaction using immunoblot analysis.

M10: Western blotting-based assay

A 9 μL of the reaction was mixed with 2X Laemmli sample buffer (cat. 1610737 Bio-Rad, CA), and then heated to 55°C for 10 minutes after we finished monitoring the ADP assay using a microplate reader. All the samples were prepared in the same manner

except for pERK2. The positive control, pERK2, was diluted to be 0.1 μM and made ready for running SDS-PAGE gel. All reactions were loaded and run on 12-well 4–20% pre-casted SDS-PAGE gel (cat. 4561095DC, Bio-Rad, CA). The proteins were transferred to a PVDF membrane (cat. 1620174, Bio-Rad, CA) and verified by blotting with 1:10,000 of p44/42 MAPK-mouse mAb (cat. 4696, CST, MA) and p7hospho-p44/42 MAPK-rabbit mAb (cat. 4370, CST, MA) respectively, followed by mouse-HRP (cat. 31430, Thermo Fisher Scientific, MA) and rabbit-HRP (cat. 7074, CST, MA). The chemiluminescent signal was detected using a CCD camera after exposing the membrane to the Western ECL Substrate (cat. 1705061, Bio-Rad, CA) for 5 minutes. This assay was repeated four times from the individual sample sets.

M11: MEK or/and ERK activity assay in-vitro Automated Assembly

For using the microfluidic printing robot, we prepared four cartridges: kinase buffer (50 mM Tris/HCl (pH 7.4), 150 mM NaCl, 10 mM $MgCl_2$, and 1 mM ATP)[30], 2.5 μM ERK2 WT substrate in the kinase buffer, 1 μM MEK1 (R4F) * in the kinase buffer, and the combination of ADP Sensor mix. We multiplexed the input reagent by printing additional droplets to the preformed one at ambient temperature. We allotted the same amount of the ADP Sensor mix but varied the concentration of the kinase proteins in each droplet. After printing four reagents with different volume ratios, the final volume of the droplet was almost 1μL. We used a fluorescence microscope to monitor the protein activity alone and the protein network reaction.

M12: Fluorescence microscope Image Acquisition and Analysis

The water-in-oil droplets on the microarray were observed under an inverted microscope (Nikon Eclipse Ti-E). For the His-tagged GFP and Cy5-streptavidin tests, a green filter cube (525 nm emission) was used to measure the GFP fluorescence and a purple filter cube (648 nm emission) was used to measure the Cy5 fluorescence. For the MEK-ERK network, a red filter cube (605 nm emission) was used to obtain the red fluorescence signals. All droplet locations were assigned, and then the droplet image was automatically taken individually at 30 °C for 1 hour every 10 min. All the microscope images were converted to a tiff image file using NIS-Elements Viewer 5.21 64-bit. The fluorescence intensities were quantitated by calculating the average red value while filtering out the black background using the OpenCV library (Python version 3.7).

Result

Printed droplet volume is consistent

To evaluate the consistency of the single droplet volume, we analyzed a single water droplet volume distribution (n=60, Figure 2b) on a PDMS substrate (Figure 2a). Specifically, 83.3% of the droplets are in the range of 52–61 nL, of which 58–61 nL droplets are the most, accounting for 40.0% of the droplets. The diameter CV (coefficient of variation) of the droplets is 2.1%, and the droplet volume CV is 6.2%. These results show the high uniformity of the single droplet, which is comparable to that of expensive piezoelectric-based droplet dispensers.[31] Therefore, the desired volume (in a discontinuous manner) can be determined by the droplet number.

To further ensure the printing stability of the microfluidic robot, we measured (Methods M6) the total weight of different droplet numbers, ranging from 100 to1000 in Figure 2c. The total droplet volume was linearly proportional to the droplet number, with a correlation coefficient of 0.9999. In particular, the slope value was 0.0592, indicating the single droplet volume was around 59.2 nL. The results showed that the microfluidic printing robot could stably print thousands of droplets, and the average droplet volume from every 100 droplets is consistent.

In addition, we tested the effect of printing pressure on droplet volume (Figure 2d). The droplet volume was increased as printing pressure increased for both water and 20% v/v glycerol-in-water, with a high correlation coefficient $R^2 = 0.9976$ and $R^2 = 0.9965$, respectively. Specifically, the water droplet volume was 62.3 nL at 2 .0 psi and 145.6 nL at 5.0 psi, and the 20% v/v glycerol-in-water volume was 57.7 Nl (7.38% decrease) at 2.0 psi and 124.8 nL (14.29% decrease) at 5.0 psi. Thus, the calibrated printing pressure for 20% v/v glycerol-in-oil was 2.2 psi for printing ~60 nL, while for water was 2.0 psi. Therefore, for most water-based reagents (e.g., PBS buffer, kinase buffer mentioned above), 2.0 psi printing pressure was used in all the following experiments.

Proteins can bind to the membrane of droplets

Next, we investigated if a functional membrane interface could be formed on each droplet. We printed five sets of droplet arrays containing 0.25 μM His-tagged GFP with different droplet sizes and added paraffin oil containing 0.5 mM Egg PE and with the different concentrations of 0, 0.0125, 0.025, 0.05, 0.1 mM DGS-NTA(Ni) (Figure 3a). As a negative control group, in the absence of DGS-NTA(Ni), green fluorescence was evenly distributed in each droplet. However, in the presence of the DGS-NTA(Ni), His-tagged GFP accumulated at the interface of the droplets. The green fluorescence signal became stronger at the interface and darker inside the droplet from left to right as the concentration of DGS-NTA(Ni) was increased from 0 to 0.1 mM. When the protein concentration is around 0.25 μM, as used in the following experiments, the results indicate that 0.1 mM is the minimal concentration of DGS-NTA(Ni) to bind almost all the His-tag proteins. However, no difference was observed by changing the droplet size, ranging from 0.24 μL to 0.96 μL, under the same concentration of DGS-NTA(Ni). Thus, these results show that the His-tagged protein immobilized at the interface of the droplet after supplementation of DGS-NTA(Ni)-containing oil over the droplets.

Next, we investigated the saturation of binding sites on the membrane interface. We studied the distribution of different concentrations of His-tagged GFP proteins under two different oils without and with DGS-NTA(Ni) (Figure 3b). We printed two sets of 0.6 μL droplet arrays containing different concentrations of GFP, ranging from 0 to 1.0 μM, and added paraffin oil containing 0.5 mM Egg PE without and with 0.1 mM DGS-NTA(Ni). In the absence of the DGS-NTA(Ni), the green fluorescence was distributed uniformly in all droplets, and the green fluorescence signal became brighter as the protein concentration increased. In the presence of the DGS-NTA(Ni), His-tagged GFP (0.25 μM) was bound at the interface. However, when the GFP concentration further increased, even with 0.1 mM DGS-NTA(Ni), the fluorescent signal inside the droplet became stronger. The result

suggests that binding sites at the interface of the droplet are limited. When the binding sites are saturated, the excess protein is distributed inside the droplet. In conclusion, when the His-tagged protein concentration is lower than 0.5 μM, most of the His-tagged proteins in the droplets are immobilized at the interface with 0.1 mM DGS-NTA(Ni).

To ensure the precise control of protein localization inside each droplet, we measured the localization of His-tagged GFP and streptavidin-Cy5. As shown in Figure 3c, we printed two sets of 6 by 6 matrices and added oils without DGS-NTA(Ni) (−Ni) and with 0.1 mM DGS-NTA(Ni) (+Ni), respectively. From the first row to the sixth row, there were 0, 1, 2, 3, 4, and 5 droplet ejections of 2.5 μM His-tagged GFP solution, and from the first column to the sixth column, there were 0, 1, 2, 3, 4 and 5 droplet ejections of 0.5 μM streptavidin-Cy5. By the additional droplet ejections of PBS buffer (pH=7.4) to the preformed droplets, each site contained 10 droplet ejections with a total volume of 0.6 μL. From all the images in Figure 3c, both the fluorescence signals from the GFP channel and the Cy5 channel gradually increased with the increased concentrations of His-tagged GFP and streptavidin-Cy5. The consistent changes of the fluorescence signals showed that our method could accurately control the two different protein concentrations in each droplet. In the case of +Ni, His-tagged GFP was immobilized at the interface of the droplet, while Streptavidin-Cy5 was distributed evenly inside the droplet. The result verifies the specificity of the binding affinity between the His-tagged proteins and DGS-NTA (Ni). Overall, our robotic platform can control the protein concentration profiles in the droplet and allow His-tagged proteins to bind to the DGS-NTA(Ni) at the membrane interface.

Well-plate assays of MEK1 (R4F) or/and ERK2 proteins

Before testing the MEK-ERK activities in droplets, we validated their kinetics using traditional well-plate and western-blot assays. As shown in Fig 4a, ATP was converted to ADP in the presence of protein kinases, then converted back to ATP in the presence of the ADP assay kit (cat. 21655, AAT Bioquest, CA).[32] The ADP assay kit detects the produced amount of the ADP indirectly through the reaction of enzyme cascades. As a result, the rate of horseradish peroxidase (HRP) activity could be measured by a fluorescent probe[32]. The ATPase activity (ATP hydrolysis) of the proteins was evaluated using a microplate reader (Method M9). A total amount of 25 μL solutions were used with 60% volume of the ADP sensor mix and 40% volume of kinase containing samples to have the final concentrations of no kinase, 0.2 μM of MEK1 (R4F)*, 0.5 μM of ERK2 WT, and the combination of both (COM) (Figure 4b). The brightest red fluorescence signal was observed in the combination group, followed by MEK1 (R4F) alone, ERK2 WT alone, and no kinase (buffer only – negative control). The red fluorescence intensity increased until it plateaued, in which the Amplex® Red concentration became limiting at the high H_2O_2 concentration or vice versa (1:1 stoichiometric ratio)[33]. ADP assay kit includes the fluorescent probe, Amplex® Red, for detecting reactive oxygen species (ROS). Once H_2O_2 was generated through the reactions initiated by the pyruvate kinase[32], converting ADP to ATP, the colorless and non-fluorescent compound, Amplex® red, reacts with H_2O_2 catalyzed by HRP, thereby forming the colored and highly fluorescent compound, resorufin[33]. Thus, the higher fluorescent intensity reflects the ATPases activity generating a larger amount of ADP. The kinase buffer group (background trace) is significantly different from other samples. 0.5 μM ERK2 WT

is significantly different from COM (0.5 μM ERK2 WT + 0.2 μM MEK1*). However, there is no significant difference between 0.5 μM ERK2 WT and 0.2 μM MEK1* and between 0.2 μM MEK1* and COM. We analyzed the data using a two-tailed *t*-test ($P < 0.05$, n=4) and a one-way ANOVA (P = 0.00023). The results proved the ATPase activity of the COM group, as well as ERK2 WT alone and MEK1 (R4F)* in the absence of the protein substrate. The ATPase activity of the single protein groups is consistent with literature data. A prior work estimated ATPase kinetic constants of phospho-MEK alone and phospho-MEK-ERK. The catalytic efficiency (k_{cat}/K_M) of phospho-MEK alone is ~ 3-fold higher than that of phospho-MEK-ERK[34]. Furthermore, the overall catalytic rate of phosphorylated ERK2 is higher than that of the unphosphorylated ERK2[35]. The combination of these two effects may explain the fastest ATP hydrolysis rate of the COM sample, but the rate was not significantly different from the MEK1*. Altogether, consistent with literature data, COM exhibits the highest ATPase activity, followed by MEK1*, and then ERK2 WT, although the concentration of MEK1* is 2.5-fold lower than ERK2 WT.

We next sought to explore the kinase activity underlying this ATPase activity right after the fluorescence read-out using western blots (Method M10). In parallel, the purified pERK2 was added next to the COM for comparison. As shown in Fig 4c, ERK2 WT was detected in the ERK2, COM, and pERK2 groups. pERk2 was identified in the COM and pERK2 groups. Thus, both ERK2 WT and phosphorylated ERK2 were detected in the COM group and the pERK2 (positive control) group, while phosphorylated ERK2 was not found in the only ERK2 sample. The western blot data demonstrated the MEK1 (R4F)-mediated phosphorylation of ERK2 in the COM group.

Kinase screening in droplets using the printing robot

We next sought to examine the ATPase activity of full-length MEK1 (R4F)* and ERK2 WT using our combinatorial droplet printer. We utilized four print heads to mix four reagents (kinase buffer, 1 μM of MEK1 (R4F) *, 2.5 μM of ERK2 WT, and ADP sensor mix) in different ratios. In each droplet, 0.6 μL out of 1 μL was allotted to the ADP sensor mix, which left 0.4 μL for multiple dilutions of protein kinase. To dilute the kinase, we printed the solutions sequentially using different amounts of kinase and kinase buffer solutions. We designed a 3 by 3 combinatorial array. Furthermore, we supplemented oil with and without 0.1 mM DGS-NTA (Ni). Oil with 0.1 mM DGS-NTA allowed selective membrane attachment of the kinases (Figure 5a). All the data were normalized within each screening assay because the ADP sensor is temperature and time sensitive. We compared the means from each concentration group to analyze the data (n=5) with a one-way ANOVA for both unbound ($P < 0.000005$, −Ni) and bound ($P < 0.00002$, +Ni) kinase categories.

We made two unique observations about the kinase assay in microliter droplets. First, the kinase concentration was not saturated in our assay because a higher concentration of both protein kinases (ERK2 WT or/and MEK1 *) produced a higher fluorescence intensity (Figure 4b and 5b). Second, our statistical analysis results confirmed the slightly higher ATPase activity in the −Ni category compared to +Ni at the same condition for all concentration groups. The results likely arise due to the diffusion limited reaction of the kinases in the localized state at the interface versus in a free state.

Otherwise, the droplet assays show consistent results with the well-plate assays. In each category, the kinase buffer (no kinase at all) showed a statistical difference from other groups that contain at least 0.1 μM MEK1 * in the −Ni category (Figure 5b, $P < 0.05$). The kinase buffer also showed a statistical difference from the COM (0.1 μM MEK1* + 0.5 μM ERK2) as well as the groups that contain at least 0.2 μM MEK1* in the +Ni category (Figure 5b, $P < 0.05$). These differences from the negative control proved the ATPase activity of ERK2 WT and MEK1 (R4F) *. The highest ATPase activity was shown in the COM (0.5 μM ERK2 + MEK1 *) without the significant difference from the only MEK1 * except 0.1 μM MEK1* in the −Ni category ($P < 0.05$). Through these results of combinatorial droplet microarray, we have demonstrated the kinase (ATPase) activity of MEK1 (R4F) * and ERK2 WT individually and together, with the selective membrane attachment of the kinases.

Conclusion

In summary, a new methodology based on the printed microdroplet platform has been developed for the high-throughput assembly and screening of a kinase pathway in vitro. The new methodology enables multiparametric studies through a few unique features (i) automated printing of microarray (ii) generation of the concentration gradient (iii) combinatorial multiplexing (iv) the microfluidic cartridges are inexpensive and disposable (cross-contamination free), (v) high printing speed/throughput in precise-controlled nanoliter droplets, (vi) it allows membrane attachment of proteins. Moreover, the new methodology endows the option of selective membrane attachment by using his6-tagged purified proteins, thus free and membrane-bound reactions could be carried out and compared in parallel. Taken together, we have demonstrated the kinase activity of MEK1 * and ERK2 WT individually and together in the multi-combinatorial microdroplet array. As a result, the difference between the ATPase assay and immunoblot assay is consistent with literature data. In a conclusion, the new methodology shows unique merits in the study of protein networks, including reaction volumes closer to the size of cells, membrane attachment flexibility, and multifactorial input-output monitoring.

Compared with multiwell-plate based protein reaction, this approach reduces the sample requirement 100-fold and allows for membrane attachment of proteins. Unlike traditional droplet-based microfluidic devices, a complex feeding structure is replaced by modular printing heads, thus greatly enhancing the utility and applicability in multifactorial protein network studies. Also, with no extra efforts (e.g., droplet sorting, trapping, and labeling), the static printed protein reactions could be monitored from input to output for at least a couple of hours. In addition, commercial automated droplet dispensers are available for combinatorial droplet-based assays. However, the cumbersome washing and cleaning processes prohibit their applications in protein studies. The use of extensive tubing and fitting connections also leads to large loading and dead volumes. In comparison with the commercial droplet dispensers, our printing cartridges are intended for disposable use. Therefore, the cross-contamination of samples between different printing sessions is greatly eliminated. Moreover, the dead volume is minimized as the reagent could be directed through the microchannels to the dispensing nozzle. These results suggest that the new

methodology could be scaled up for screening protein network activities with multi-kinases forming the signaling pathway in artificial cells.

As a new method to reconstitute protein networks, more complex protein kinase reactions could be studied to better understand their reaction mechanisms and crosstalk. Furthermore, drug actions could be further studied using the reconstituted protein networks. Therefore, our work may enable the systematic and high-throughput study of other biochemical pathways for drug discovery. We note that biomolecules could be absorbed by the reservoir layer, altering the concentrations and viscosity of the reagent. In such cases, surface passivation treatment may be required along with the selection of proper reservoir material. In pursuit of higher throughput, microfluidic printing robots can be integrated with standard microscopy instruments, allowing alternate printing and reaction monitoring. One limitation of our system is the manual volume calibration of different reagents. Calibration automation may be implemented to improve printing accuracy and efficiency.

Acknowledgements

This research work was partially supported by NIH (5R21EB025938), Joint Research Fund for Overseas Chinese Scholars and Scholars in Hong Kong and Macao (No.51929501), the Strategic Priority Research Program of the Chinese Academy of Sciences (XDA16021303), the Guangdong Program (2016ZT06D631), and Shenzhen Engineering Laboratory of Single-Molecule Detection and Instrument Development (XMHT20190204002). The authors appreciate Dr. John Albeck and Dr. Atul Parikh for their advice and suggestions on the project.

Reference

(1). dos Santos EC; Belluati A; Necula D; Scherrer D; Meyer CE; Wehr RP; Lörtscher E; Palivan CG; Meier W Combinatorial Strategy for Studying Biochemical Pathways in Double Emulsion Templated Cell-Sized Compartments. Adv. Mater 2020, 32 (48). 10.1002/adma.202004804.

(2). Garni M; Einfalt T; Goers R; Palivan CG; Meier W Live Follow-Up of Enzymatic Reactions Inside the Cavities of Synthetic Giant Unilamellar Vesicles Equipped with Membrane Proteins Mimicking Cell Architecture. ACS Synth. Biol 2018, 7 (9). 10.1021/acssynbio.8b00104.

(3). Hui E; Vale RD *In Vitro* Membrane Reconstitution of the T-Cell Receptor Proximal Signaling Network. Nat. Struct. Mol. Biol 2014. 10.1038/nsmb.2762.

(4). Su X; Ditlev JA; Hui E; Xing W; Banjade S; Okrut J; King DS; Taunton J; Rosen MK; Vale RD Phase Separation of Signaling Molecules Promotes T Cell Receptor Signal Transduction. Science (80-.). 2016. 10.1126/science.aad9964.

(5). Miller TE; Beneyton T; Schwander T; Diehl C; Girault M; McLean R; Chotel T; Claus P; Cortina NS; Baret JC; Erb TJ Light-Powered CO2 Fixation in a Chloroplast Mimic with Natural and Synthetic Parts. Science (80-.). 2020, 368 (6491). 10.1126/science.aaz6802.

(6). Berhanu S; Ueda T; Kuruma Y Artificial Photosynthetic Cell Producing Energy for Protein Synthesis. Nat. Commun 2019. 10.1038/s41467-019-09147-4.

(7). Cui N; Zhang H; Schneider N; Tao Y; Asahara H; Sun Z; Cai Y; Koehler SA; De Greef TFA; Abbaspourrad A; Weitz DA; Chong S A Mix-and-Read Drop-Based *in Vitro* Two-Hybrid Method for Screening High-Affinity Peptide Binders. Sci. Rep 2016. 10.1038/srep22575.

(8). Wang D; Gou SY; Axelrod D Reaction Rate Enhancement by Surface Diffusion of Adsorbates. Biophys. Chem 1992, 43 (2). 10.1016/0301-4622(92)80027-3.

(9). Gureasko J; Galush WJ; Boykevisch S; Sondermann H; Bar-Sagi D; Groves JT; Kuriyan J Membrane-Dependent Signal Integration by the Ras Activator Son of Sevenless. Nat. Struct. Mol. Biol 2008, 15 (5). 10.1038/nsmb.1418.

(10). Mazutis L; Baret JC; Treacy P; Skhiri Y; Araghi AF; Ryckelynck M; Taly V; Griffiths AD Multi-Step Microfluidic Droplet Processing: Kinetic Analysis of an in Vitro Translated Enzyme. Lab Chip 2009, 9 (20). 10.1039/b907753g.

(11). Srisa-Art M; Dyson EC; DeMello AJ; Edel JB Monitoring of Real-Time Streptavidin-Biotin Binding Kinetics Using Droplet Microfluidics. Anal. Chem 2008, 80 (18). 10.1021/ac801199k.

(12). Cai LF; Zhu Y; Du GS; Fang Q Droplet-Based Microfluidic Flow Injection System with Large-Scale Concentration Gradient by a Single Nanoliter-Scale Injection for Enzyme Inhibition Assay. Anal. Chem 2012, 84 (1). 10.1021/ac2029198.

(13). Agresti JJ; Antipov E; Abate AR; Ahn K; Rowat AC; Baret JC; Marquez M; Klibanov AM; Griffiths AD; Weitz DA Ultrahigh-Throughput Screening in Drop-Based Microfluidics for Directed Evolution. Proc. Natl. Acad. Sci. U. S. A 2010, 107 (9). 10.1073/pnas.0910781107.

(14). Sun S; Slaney TR; Kennedy RT Label Free Screening of Enzyme Inhibitors at Femtomole Scale Using Segmented Flow Electrospray Ionization Mass Spectrometry. Anal. Chem 2012, 84 (13). 10.1021/ac3011389.

(15). Huebner A; Bratton D; Whyte G; Yang M; Demello AJ; Abell C; Hollfelder F Static Microdroplet Arrays: A Microfluidic Device for Droplet Trapping, Incubation and Release for Enzymatic and Cell-Based Assays. Lab Chip 2009, 9 (5). 10.1039/b813709a.

(16). Sun M; Bithi SS; Vanapalli SA Microfluidic Static Droplet Arrays with Tuneable Gradients in Material Composition. Lab Chip 2011, 11 (23). 10.1039/c1lc20709a.

(17). Chen X; Ren CL A Microfluidic Chip Integrated with Droplet Generation, Pairing, Trapping, Merging, Mixing and Releasing. RSC Adv. 2017, 7 (27). 10.1039/c7ra02336g.

(18). Wang X; Liu X; Huang X Bioinspired Protein-Based Assembling: Toward Advanced Life-Like Behaviors. Adv. Mater 2020. 10.1002/adma.202001436.

(19). Shim J; Zhou C; Gong T; Iserlis DA; Linjawi HA; Wong M; Pan T; Tan C Building Protein Networks in Synthetic Systems from the Bottom-Up. Biotechnol. Adv 2021, 49, 107753. 10.1016/j.biotechadv.2021.107753. [PubMed: 33857631]

(20). Rane TD; Zec HC; Wang TH A Barcode-Free Combinatorial Screening Platform for Matrix Metalloproteinase Screening. Anal. Chem 2015, 87 (3). 10.1021/ac504330x.

(21). Abate AR; Hung T; Marya P; Agresti JJ; Weitz DA High-Throughput Injection with Microfluidics Using Picoinjectors Using Picoinjectors. Proc. Natl. Acad. Sci. U. S. A 2010, 107 (45). 10.1073/pnas.1006888107.

(22). Weiss M; Frohnmayer JP; Benk LT; Haller B; Janiesch JW; Heitkamp T; Börsch M; Lira RB; Dimova R; Lipowsky R; Bodenschatz E; Baret JC; Vidakovic-Koch T; Sundmacher K; Platzman I; Spatz JP Sequential Bottom-up Assembly of Mechanically Stabilized Synthetic Cells by Microfluidics. Nat. Mater 2018. 10.1038/NMAT5005.

(23). Cole RH; Tang SY; Siltanen CA; Shahi P; Zhang JQ; Poust S; Gartner ZJ; Abate AR Printed Droplet Microfluidics for on Demand Dispensing of Picoliter Droplets and Cells. Proc. Natl. Acad. Sci. U. S. A 2017, 114 (33). 10.1073/pnas.1704020114.

(24). Wang J; Deng K; Zhou C; Fang Z; Meyer C; Deshpande KUA; Li Z; Mi X; Luo Q; Hammock BD; Tan C; Chen Y; Pan T Microfluidic Cap-To-Dispense (MCD): A Universal Microfluidic-Robotic Interface for Automated Pipette-Free High-Precision Liquid Handling. Lab Chip 2019, 19 (20), 3405–3415. 10.1039/c9lc00622b. [PubMed: 31501848]

(25). Sivashankar S; Agambayev S; Buttner U; Salama KN Characterization of Solid UV Curable 3D Printer Resins for Biological Applications. In 2016 IEEE 11th Annual International Conference on Nano/Micro Engineered and Molecular Systems, NEMS 2016; 2016. 10.1109/NEMS.2016.7758255.

(26). Lepowsky E; Amin R; Tasoglu S Assessing the Reusability of 3D-Printed Photopolymer Microfluidic Chips for Urine Processing. Micromachines 2018, 9 (10). 10.3390/mi9100520.

(27). Mata A; Fleischman AJ; Roy S Characterization of Polydimethylsiloxane (PDMS) Properties for Biomedical Micro/Nanosystems. Biomed. Microdevices 2005, 7 (4). 10.1007/s10544-005-6070-2.

(28). Robbins DJ; Zhen E; Owaki H; Vanderbilt CA; Ebert D; Geppert TD; Cobb MH Regulation and Properties of Extracellular Signal-Regulated Protein Kinases 1 and 2 in Vitro. J. Biol. Chem 1993, 268 (7).

(29). Khokhlatchev A; Xu S; English J; Wu P; Schaefer E; Cobb MH Reconstitution of Mitogen-Activated Protein Kinase Phosphorylation Cascades in Bacteria. Efficient Synthesis of Active Protein Kinases. J. Biol. Chem 1997, 272 (17). 10.1074/jbc.272.17.11057.

(30). Pirman NL; Barber KW; Aerni HR; Ma NJ; Haimovich AD; Rogulina S; Isaacs FJ; Rinehart J A Flexible Codon in Genomically Recoded Escherichia Coli Permits Programmable Protein Phosphorylation. Nat. Commun 2015, 6. 10.1038/ncomms9130.

(31). Fan J; Men Y; Hao Tseng K; Ding Y; Ding Y; Villarreal F; Tan C; Li B; Pan T Dotette: Programmable, High-Precision, Plug-and-Play Droplet Pipetting. Biomicrofluidics 2018, 12 (3). 10.1063/1.5030629.

(32). Lian Q; Cao H; Wang F The Cost-Efficiency Realization in the Escherichia Coli-Based Cell-Free Protein Synthesis Systems. Appl. Biochem. Biotechnol 2014, 174 (7), 2351–2367. 10.1007/s12010-014-1143-4. [PubMed: 25185501]

(33). Zhao B; Summers FA; Mason RP Photooxidation of Amplex Red to Resorufin: Implications of Exposing the Amplex Red Assay to Light. Free Radic. Biol. Med 2012, 53 (5). 10.1016/j.freeradbiomed.2012.06.034.

(34). Rominger CM; Schaber MD; Yang J; Gontarek RR; Weaver KL; Broderick T; Carter L; Copeland RA; May EW An Intrinsic ATPase Activity of Phospho-MEK-1 Uncoupled from Downstream ERK Phosphorylation. Arch. Biochem. Biophys 2007, 464 (1), 130–137. 10.1016/j.abb.2007.04.004. [PubMed: 17490600]

(35). Wang ZX; Zhou B; Wang QM; Zhang ZY A Kinetic Approach for the Study of Protein Phosphatase-Catalyzed Regulation of Protein Kinase Activity. Biochemistry 2002, 41 (24), 7849–7857. 10.1021/bi025776m. [PubMed: 12056917]

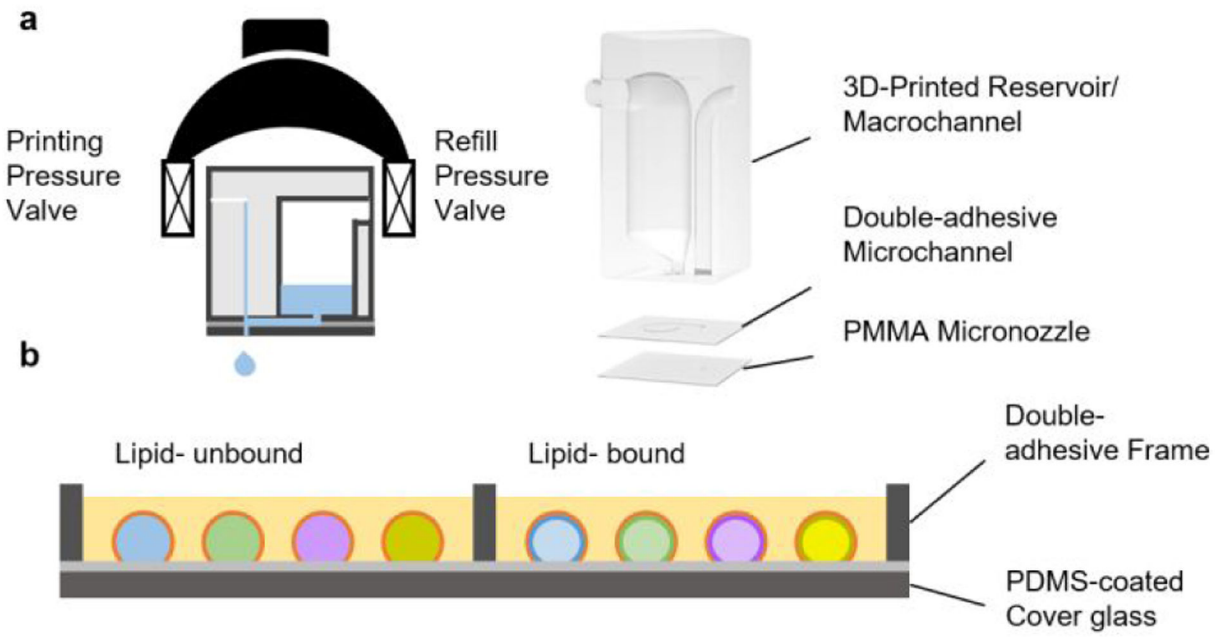

Figure 1. Formation of multiplexed microdroplet arrays.

a) Illustration of the microfluidic printing was operated by a two-finger robot equipped with pneumatic controllers, and the printing head consists of a 3D-printed reservoir/macrochannel layer, a double-adhesive microchannel layer, and a PMMA micronozzle layer. b) Egg PE-containing oil, w/o (Left) and w/ (Right) anchor lipids DGS-NTA(Ni), are added onto the microdroplet arrays.

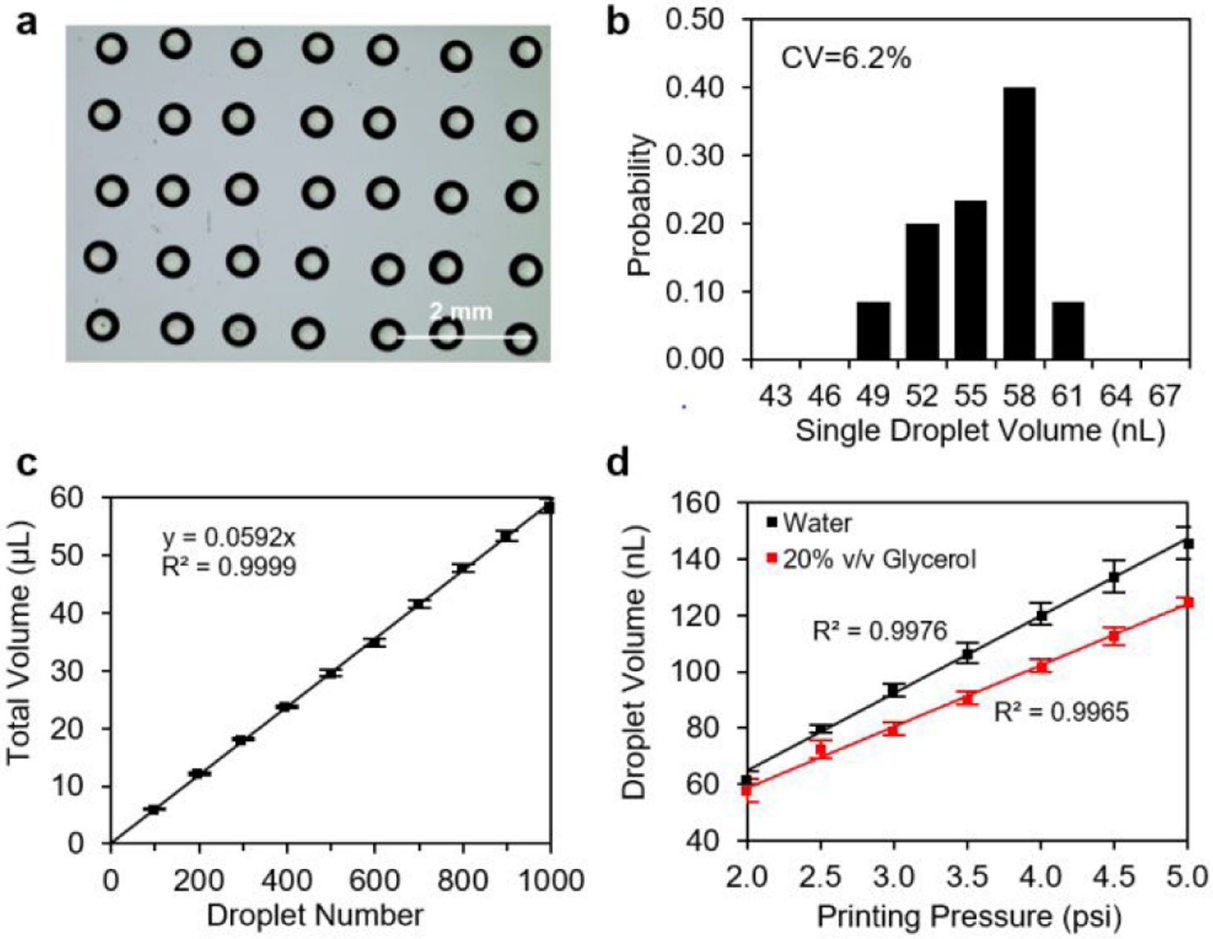

Figure 2. Validation of printed droplets by the microfluidic printing robot.

a) The microscopic image of a droplet array; b) the single droplet volume distribution (n=60); c) linearity of the total droplet volume of 100–1000 droplets, with a $R^2 > 0.9999$; d) the averaged single droplet volume under various printing pressure from 2.0 to 5.0 psi. Black indicates water droplet. Red indicates 20% v/v glycerol droplet.

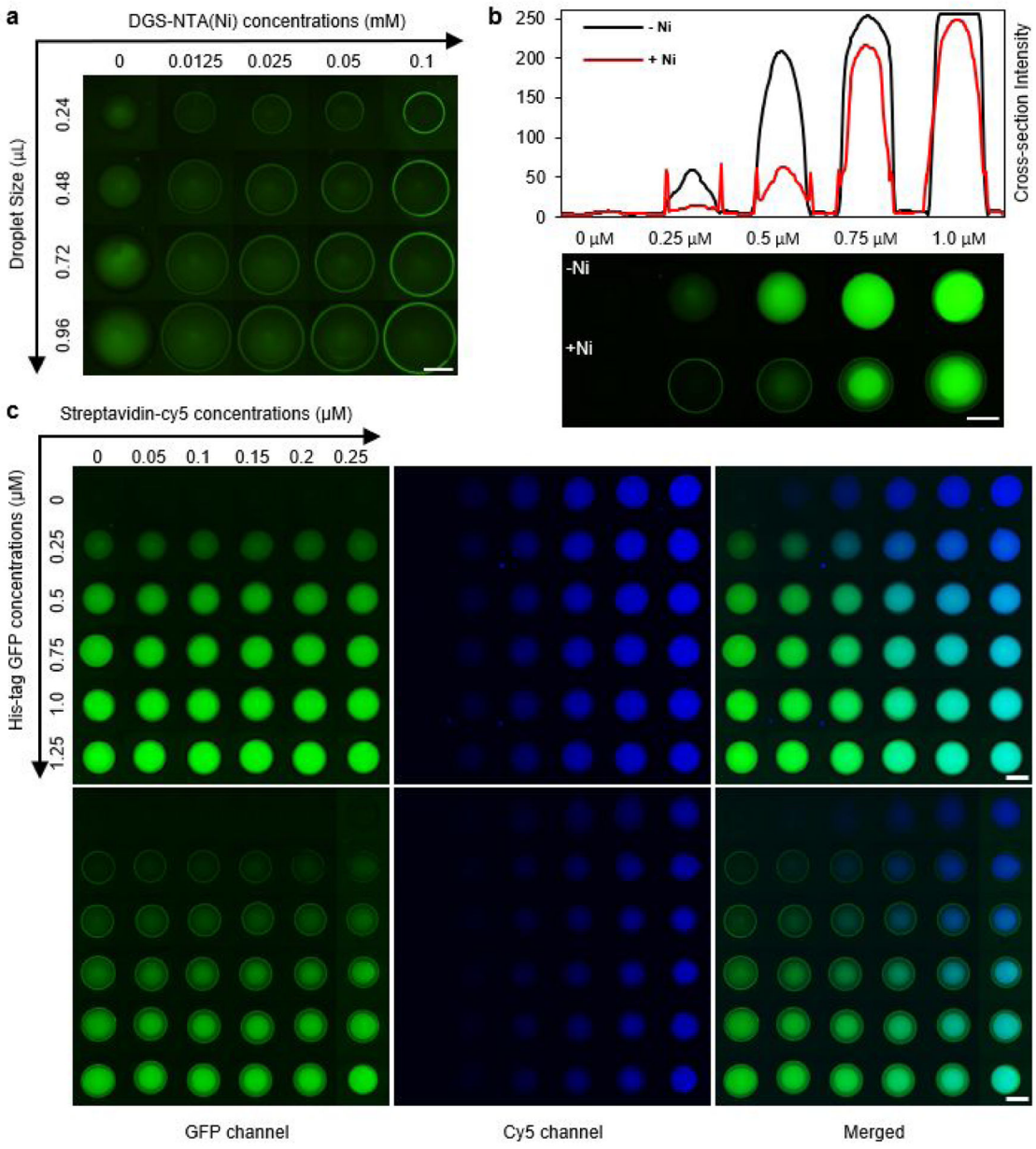

Figure 3. Printed droplet arrays using fluorescent probes.

a) Fluorescent images of 0.24, 0.48, 0.72 and 0.96 μL droplets containing 0.25 μM His-tag GFP under 0, 0.0125, 0.025, 0.05, 0.1 mM DGS-NTA(Ni); b) Fluorescent images and cross-section fluorescent intensities of 0.48 μL droplets containing 0, 0.25, 0.5, 0.75 and 1.0 μM His-tag GFP under 0 (black curve) and 0.1 mM (red curve) DGS-NTA(Ni); c) GFP channel, Cy5 channel and Merged (GFP and Cy5) results from the combinatorial droplet array with His-tag GFP (0–1.25 μM), streptavidin-Cy5 (0–0.25 μM), and PBS buffer (pH=7.4) under 0 (Top, −Ni) and 0.1 mM (Bottom, +Ni) DGS-NTA(Ni). Scale bar: 500 μM. (GPF images: 1s exposure time, Cy5 images: 500 ms exposure time).

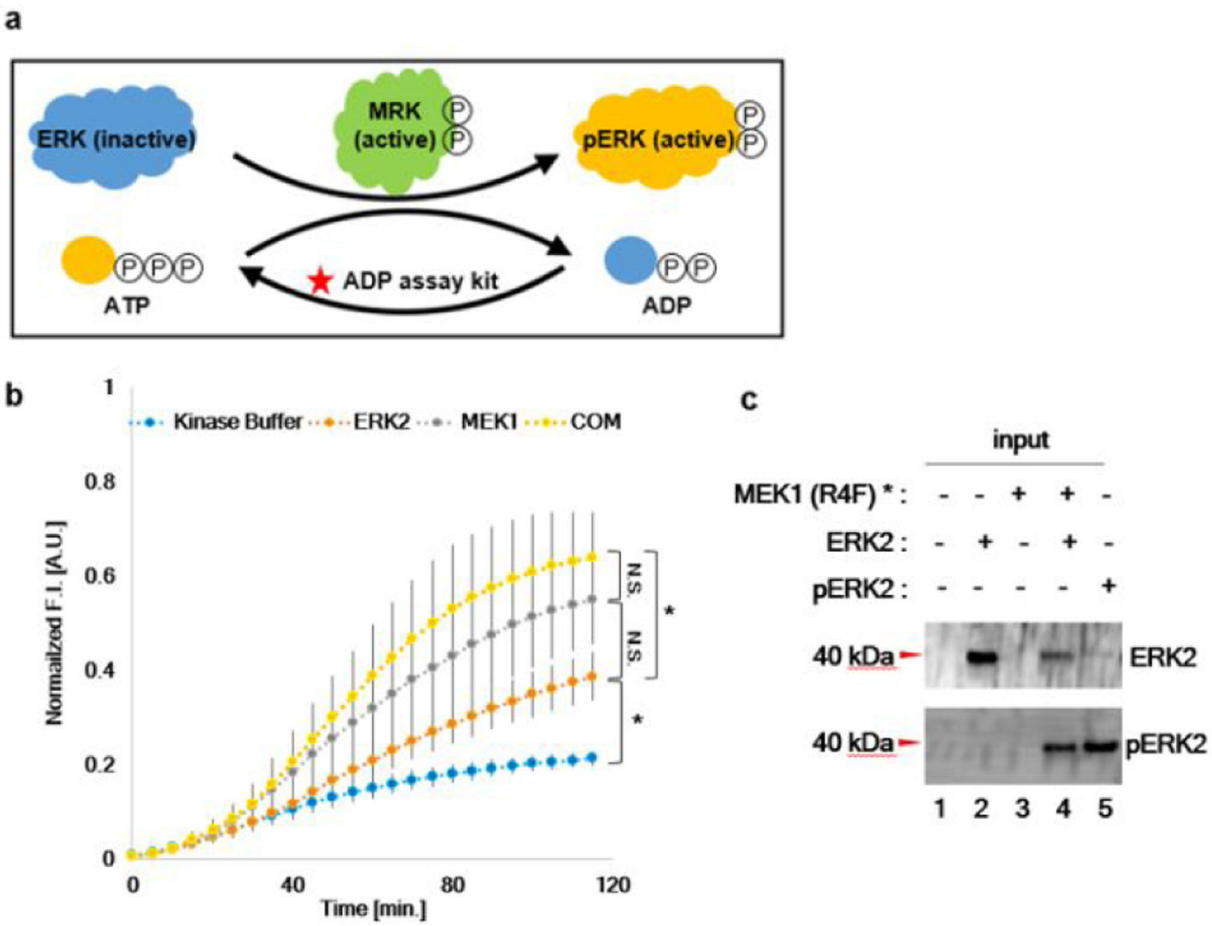

Figure 4. Validation of MEK-ERK activities in well-plate assays.

a) Schematic diagram of the MEK-ERK protein network activities; b) The ATPase activities were examined using a microplate reader. Error bars represent ±SD from the mean of four independent experiments (n = 4). Two tailed *t*-test (*, $P < 0.05$; significance difference between two groups, N.S.; no significant difference); c) Immunoblot analysis of proteins with antibodies against indicated kinase proteins. The cropped panels were taken from the same reaction after the fluorescence signal read-out in b.

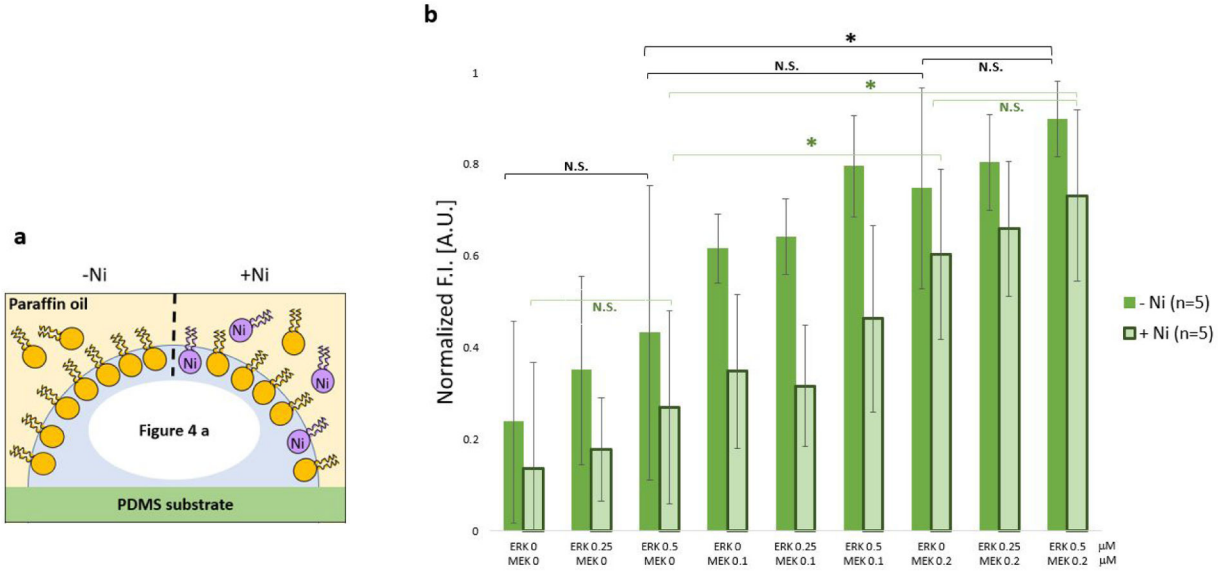

Figure 5. Validation of MEK-ERK activities in droplets with and without membranes.

a) Schematic illustration of the water in oil droplet included reactions without (−Ni) and with 0.1 mM DGS-NTA (Ni) (+Ni). b) ADP screening results. Normalized F.I. from two-dimensional dilution of both ERK2 WT and MEK1 * without (−Ni) and with 0.1 mM DGS-NTA (Ni) (+Ni).